



Electrochemical performance of TiCN coatings with low carbon concentration in simulated body fluid



Qianzhi Wang^{a,b,c}, Fei Zhou^{a,b,*}, Zhifeng Zhou^d, Lawrence Kwok-Yan Li^d, Jiwang Yan^c

^a State Key Laboratory of Mechanics and Control of Mechanical Structures, Nanjing University of Aeronautics and Astronautics, Nanjing 210016, China

^b College of Mechanical and Electrical Engineering, Nanjing University of Aeronautics and Astronautics and Jiangsu Key Laboratory of Precision and Micro-Manufacturing Technology, Nanjing 210016, China

^c Department of Mechanical Engineering, Faculty of Science and Technology, Keio University, Hiyoshi 3-14-1, Kohoku-ku, Yokohama 223-8522, Japan

^d Advanced Coatings Applied Research Laboratory, Department of Mechanical and Biomedical Engineering, City University of Hong Kong, 83 Tat Chee Avenue, Kowloon, Hong Kong, China

ARTICLE INFO

Article history:

Received 22 March 2014

Accepted in revised form 12 May 2014

Available online 27 May 2014

Keywords:

Sputtered coatings

Electrochemistry

Impedance

Polarization

Simulated body fluid

ABSTRACT

TiCN coatings with low carbon concentrations (0.99 at.%–2.46 at.%) were deposited on Si(100) wafers via co-sputtering titanium and graphite targets by using unbalanced magnetron sputtering. The influence of carbon content on the microstructure and electrochemical properties of TiCN coatings in simulated body fluid was analyzed. The results revealed that the amorphous carbon (a-C) was absent from TiCN coatings (0.99 at.% or 2.05 at.% carbon), which exhibited favorable corrosion resistances in SBF. But the presence of a-C in TiCN coating (2.46 at.% carbon) lowered its hardness, and subsequently deteriorated its corrosion resistance in SBF. In particular, the TiCN coating with 2.05 at.% carbon presented the higher charge transfer resistance (R_{ct}) as compared with the TiCN coating (0.99 at.% carbon) owing to more a-CN_x and higher electrical resistivity.

© 2014 Elsevier B.V. All rights reserved.

1. Introduction

Owing to low cost, non-magnetic and easy hot and cold workability, the 316L austenitic stainless steel is used widely as surgical prosthesis replacement [1,2]. Nevertheless, approximately 10% of hip arthroplasties need be replaced after 10–15 years due to local corrosion, which resulted from the high Cl⁻ concentration and moderate temperature of human body fluid [3–11]. In addition, the release of iron and nickel ions from 316L stainless steel may cause permanent implant's failure because of the formation of fibrous tissue [12–15]. Thus, many researchers have focused on the deposition of different anti-corrosion coatings on the 316L stainless steels. Currently, TiCN coatings have been concerned due to lower internal stress, higher hardness and superior tribological property [16–21]. As seen in Table 1, the nanocomposite TiN/a-C coatings exhibited better corrosion protection than single layer TiN coatings owing to small crystallite size, reduced micro-porosity and dense microstructure [22], while Antunes et al. [23] pointed out that the anti-corrosion ability of TiCN-coated 316L with many defects was even inferior to bare 316L. Moreover, the corrosion current density (0.175 $\mu\text{A}/\text{cm}^2$) of C-TiN coating was higher than that (0.168 $\mu\text{A}/\text{cm}^2$) of H₂-TiN coating [24]. Thus, the above-mentioned conflicting results may be closely related to carbon concentration in TiCN coatings, but the carbon concentration was either not reported or was constant in

Refs. [22–24]. For TiCN coatings with different carbon concentrations, Senna et al. [25] claimed that the corrosion resistances of TiCN coatings became poor with increasing carbon concentration due to the high density of defects, but Liu et al. [26] demonstrated that Ti/a-CN_x coatings with less amorphous carbon exhibited better anti-corrosion property. Therefore, it is concluded that TiCN coatings with low carbon concentration could possess favorable corrosion resistance. However, up to now, no papers focused on the electrochemical properties of TiCN coatings with low carbon concentration (<3.0 at.%). Thus, it is imperative to study the electrochemical performance of TiCN coatings with low carbon concentration.

In this study, to obtain the excellent electrochemical performance of TiCN coatings, TiCN coatings with different low carbon concentrations were deposited on Si(100) wafers. The electrochemical behavior of Si wafers coated with TiCN coatings in SBF was investigated simultaneously via open circuit potential (OCP), electrochemical impedance spectroscopy (EIS) and potentiodynamic polarization test, respectively. Then, the influence of carbon concentration on the microstructure and electrochemical characteristic of TiCN coating in SBF was discussed.

2. Experiment details

2.1. Deposition and characterizations of TiCN coatings

Monocrystalline Si(100) wafers were used as substrates and ultrasonically cleaned in ethanol and deionized water in succession. Prior

* Corresponding author. Tel./fax: +86 25 84893083.
E-mail address: fzhou@nuaa.edu.cn (F. Zhou).

Table 1
Conditions of electrochemical tests for TiCN coatings in different references.

References	Coatings	Substrate	Electrolyte	Temperature	C concentration	Amorphous carbon
Harish [22]	TiN/a-C	M3 tool steel	0.5 M HCl solution	Room temperature	No report	Presence
Antunes [23]	TiCN	316L	Hank's solution	37 °C	No report	No measurement
Sofiane [24]	C-TiN	Titanium	Simulated body fluid	37 °C	= 8.01 at.%	Presence
Senna [25]	TiCN	M2 HSS	0.5 M Na ₂ SO ₄ solution (pH 5.5)	Room temperature	> 18.8 at.%	No measurement
Liu [26]	Ti/a-CN _x	Ti6Al4V	Tyrode's solution (pH 7.4)	37 °C	No report	Presence

to coating deposition, Si(100) wafers were further cleaned with Ar⁺ plasma at a bias voltage of −450 V for 30 min, and then TiCN coatings were deposited using unbalanced magnetron sputtering (UDP-650, Teer Coatings Limited, UK) via co-sputtering pure titanium and graphite targets with a mixed atmosphere of Ar and N₂ gases. In order to increase the adhesive strength between TiCN coating and Si(100) wafer, a pure Ti adhesive layer (about 0.2 μm) was deposited onto Si substrate in advance. During coating deposition, chamber pressure was maintained at 0.23 GPa while bias voltage and rotational speed of holder were kept at −60 V and 10 rpm. The carbon concentration in TiCN coatings was controlled via adjusting graphite target current from 1 A to 3 A while titanium target current was kept at 8 A. The TiCN coatings deposited at graphite target current of 1 A, 2 A and 3 A were denoted as TiCN(1), TiCN(2) and TiCN(3) coatings, and the pure TiN coating was also deposited on Si(100) wafer for comparison.

The thicknesses and element concentration of TiCN coatings were determined using field emission scanning electron microscope (FE-SEM) (Philips FEG-XL30) equipped with EDS (Inca Energy 350, Oxford, UK), while their phase and bonding structure were characterized using Raman spectroscopy with wavelength of 633 nm (InVia 2000, Renishaw), X-ray diffraction (XRD, D8-Advance, Bruker, Germany) with Cu Kα radiation (λ = 0.15404 nm) and X-ray photoelectron spectroscopy (XPS, VG ESCALAB 220-iXL Al Kα), respectively. The XPS spectra were deconvoluted via XPS PEAK 4.1 software with the reference C_{1s} peak at 284.8 eV. The electrical resistivity and hardness of TiCN coatings were measured using a four point probe technique (KDY-1, KunDe Technology Co., LTD) and Nano Indenter XP (Nano Instruments; Inc., Oak Ridge, Tennessee).

Table 2
Chemical composition of simulated body fluid.

Compound	Concentration (g/L)
NaCl	7.996
NaHCO ₃	0.350
KCl	0.220
K ₂ HPO ₄ ·3H ₂ O	0.228
MgCl ₂ ·6H ₂ O	0.305
CaCl ₂	0.278
Na ₂ SO ₄	0.071
(CH ₂ OH) ₃ CNH ₂	6.057
1 mol/L HCl	For pH controlling

Table 3
Element concentrations, thicknesses, hardnesses and electrical resistivities of TiN and TiCN coatings.

Samples	Ti (at.%)	C (at.%)	N (at.%)	Thickness (μm)	Hardness (GPa)	Electrical resistivity (Ω·mm ² /m)
TiN	46.42	–	53.58	1.14	20 ± 1.2	0.86
TiCN(1)	48.66	0.99	50.35	1.24	32 ± 2.8	1.44
TiCN(2)	48.31	2.05	49.64	1.15	31 ± 1.9	1.68
TiCN(3)	50.36	2.46	47.18	1.24	29 ± 3.1	2.87

2.2. Characterization of electrochemical corrosion behavior

Prior to electrochemical tests, the TiCN-coated Si(100) wafers were first connected with copper wires by conductive graphite glue, and then enveloped by 704 silicon rubber with 1 × 1 cm² exposing area. The electrochemical measurements were performed using a standard three-electrode electrochemical cell which has been described elsewhere [27]. Simulated body fluid (SBF) was used as electrolyte with pH 7.4, and its detailed concentration is listed in Table 2 [28]. The open circuit potential (OCP) measurement was immediately begun after the specimen was immersed in SBF. When the OCP measurement had been done for 1 h, the electrochemical impedance spectroscopy (EIS) was performed at OCP with an AC excitation of 10 mV over the frequency range from 1 MHz to 100 kHz. Subsequently, the potentiodynamic polarization test was carried out via polarizing specimen in the

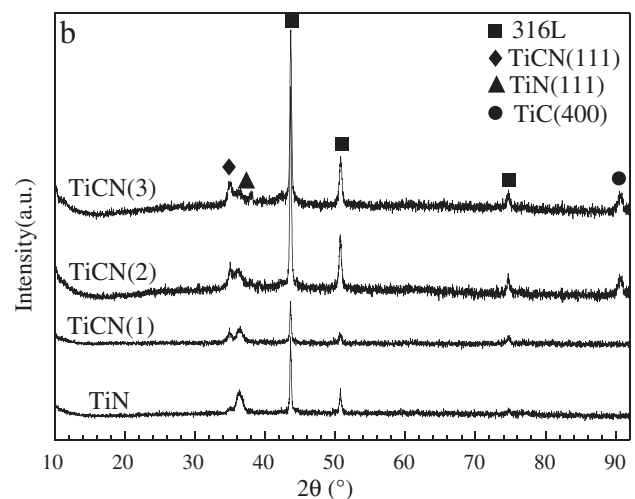
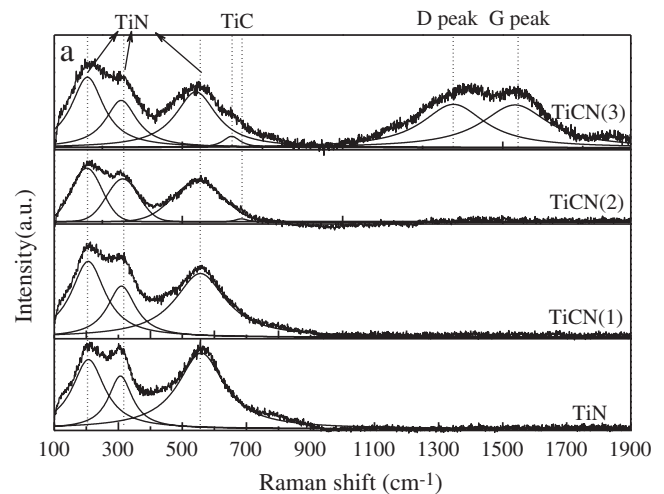


Fig. 1. (a) Raman spectra and (b) XRD of TiN and TiCN coatings deposited at different graphite target currents.

anodic direction from -0.8 V to 0.8 V with a sweep rate at 20 mV/min. All above-mentioned measurements were carried out at 37°C controlled by water bath kettle (DF-101S), and repeated for three times. Subsequently, EIS data were illustrated in the form of Nyquist and Bode plots, and fitted with equivalent circuit using ZsimpWin software. After potentiodynamic polarization test, corrosion potential (E_{corr}) and corrosion current density (j_{corr}) were deduced from the Tafel plot with extrapolation method, and then polarization resistance (R_p) was obtained using Stern-Geary Eq. (1) [29,30].

$$R_p = \frac{\beta_a \beta_c}{2.303 j_{\text{corr}} (\beta_a + \beta_c)} \quad (1)$$

where the β_a and β_c are the Tafel anodic and cathodic slopes.

3. Results and discussion

3.1. Characterizations of TiCN coatings

According to EDS analysis, each element concentration of TiCN coatings is listed in Table 3. As the graphite target current increased from 1 A to 3 A, the concentration of C atom increased gradually from 0.99 at.% to 2.46 at.% while that of N atom decreased from 50.35 at.% to 47.18 at.%. Although the concentrations of Ti atoms in TiCN coatings increased slightly, the numerical values were all higher than that of TiN coating

Table 4
Volume fractions of different bonds from N_{1s} XPS results of TiCN coatings.

Coatings	N–Ti–O (%)	N–Ti (%)	N–C (%)	N = C (%)
TiCN(1)	30.2	44.3	8.4	17.1
TiCN(2)	28.2	42.2	3.7	25.9
TiCN(3)	22.0	35.5	4.7	37.8

after carbon doping. It implies that C atom was easier to bond with Ti atom rather than N atom.

As seen in Fig. 1a, the Raman spectra of TiN and TiCN(1) coatings could be fitted into three peaks related to TiN phases at 218 , 311 and 556 cm^{-1} [31]. However, when the graphite target current exceeded 1 A, the novel peaks located around 674 cm^{-1} appeared simultaneously in Raman spectra of TiCN(2) and TiCN(3) coatings which manifest the formations of TiC [31]. Moreover, the Raman spectrum of TiCN(3) coating exhibited the obvious D (disordered carbon) and G (graphitic carbon) peaks centered at around 1350 and 1580 cm^{-1} generally [32]. This indicated that the C in TiCN(3) coating was not only bonded with Ti, but also redundant to form amorphous carbon [33]. As seen in Fig. 1b, TiC(400) diffraction peaks were observed in XRD of TiCN(2) and TiCN(3) coatings which is agreement with the results of Raman analysis [21]. Moreover, as graphite target current increased from 1 A to 3 A, the intensity of TiN(111) diffraction peak decreased while that of TiCN(111) diffraction peak increased gradually [19]. It implied that the position of N atom in TiN lattice was replaced by C atom in the form of solid solution.

Fig. 2 showed Ti_{2p} and N_{1s} XPS spectra of TiCN coatings. After carbon was doped, the Ti–N–O bond at 457 eV in TiN coating was shifted to Ti–(N,C) bond in the range of 456.6 – 456.9 eV [31,34], which is consistent with the appearance of TiCN peak in XRD. The similar variation trend exhibited in N_{1s} XPS spectra in Fig. 2b, i.e., the N–Ti bond at 397.2 eV was transferred to N–Ti–C bond at 396.8 eV [34,35]. In order to understand the detailed bonding structures of TiCN coatings, the volume fractions of different bonds were calculated and listed in Table 4. It is clear that the volume fraction of N–Ti bond decreased gradually while that of the N=C bond increased from 17.1% to 37.8% simultaneously. Thus, taking the Raman, XRD and XPS analyses into account, the compositions of TiN(TiCN) coatings transferred from TiN to TiN, Ti(C,N), a-CN_x, and then to TiN, Ti(C,N), TiC, a-CN_x, a-C. Since the electrical resistivity (10^8 Ω cm) of a-CN_x was higher than that (2.7×10^5 – 3.7×10^7 Ω cm) of TiN [36,37]. Thus, under the effect of bonding variation, in particular the increasing content of a-CN_x, the electrical resistivity in Table 3 increased from 0.86 $\Omega \cdot \text{mm}^2/\text{m}$ for TiN coating to 2.87 $\Omega \cdot \text{mm}^2/\text{m}$ for TiCN(3) coating.

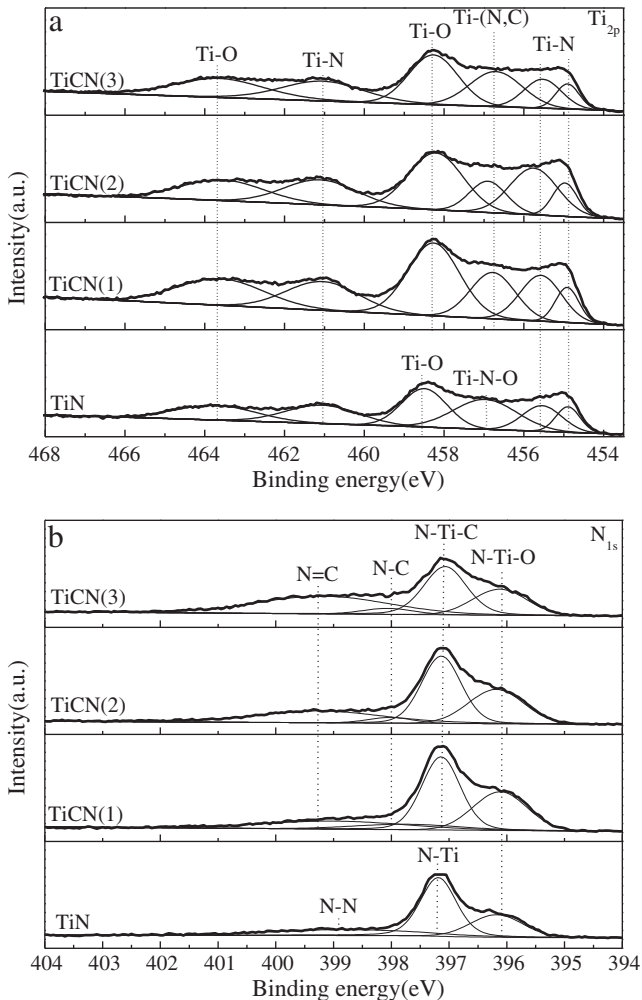


Fig. 2. Ti_{2p} and N_{1s} XPS spectra of TiN and TiCN coatings deposited at different graphite target currents.

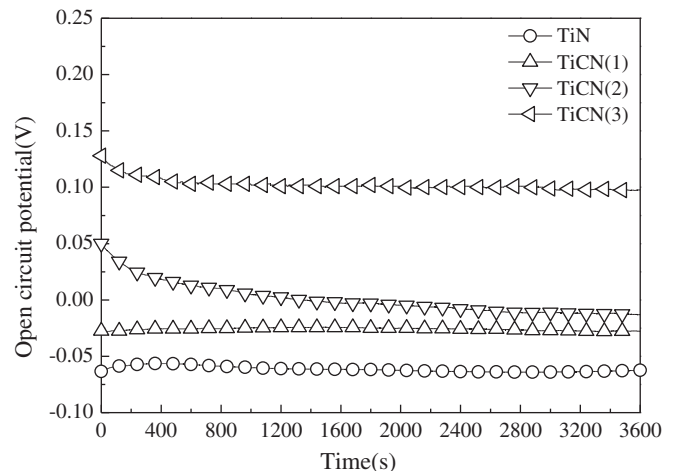


Fig. 3. OCPs of TiN and TiCN coatings deposited at different graphite target currents.

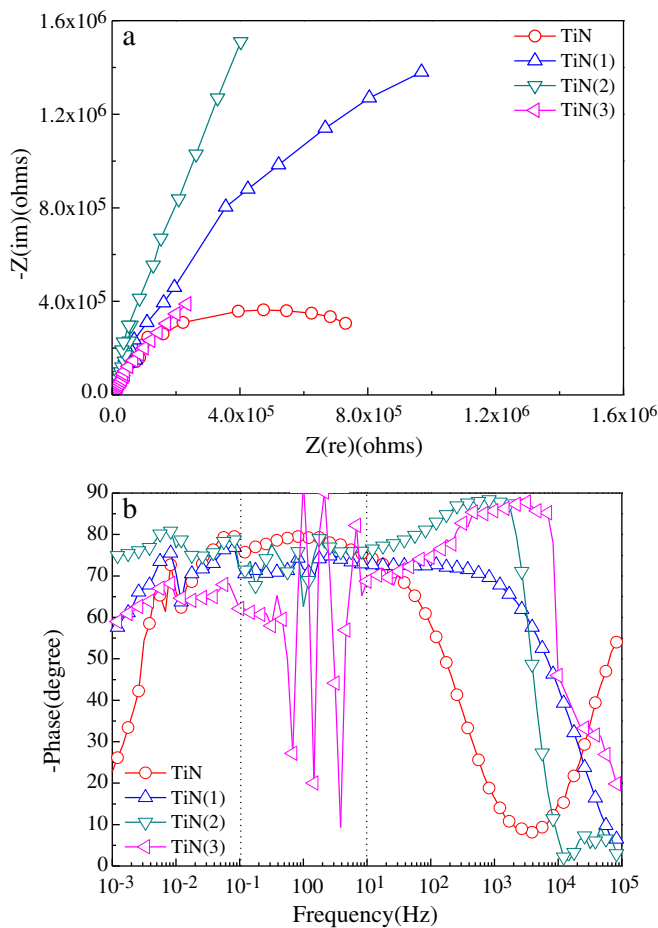


Fig. 4. (a) Nyquist plots (b) Bode plots as a function of frequency of TiN and TiCN coatings deposited at different graphite target currents.

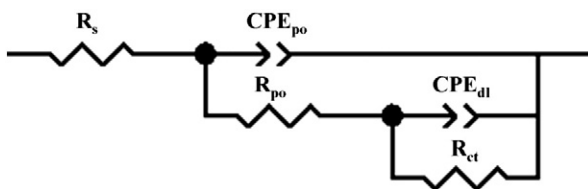


Fig. 5. Equivalent circuit of TiN and TiCN coatings.

The hardness of TiCN coatings is listed in Table 3. Obviously, the TiN coating presented the lowest hardness of 20 GPa while those of the TiCN coatings all increased after carbon doping. However, when the graphite target current increased from 1 A to 3 A, the hardness of TiCN coatings decreased from 32 GPa to 29 GPa with a reduction of 3 GPa. This is owing to the formations of amorphous carbon nitride and amorphous carbon in coatings, which acted as defects in the TiCN coatings [18,21]. In addition, the standard deviation of hardness for TiCN(3) coating

increased sharply to 3.1 GPa as compared with 1.9 GPa for TiCN(2) coating. Thus, it is well proved that the density of the TiCN(3) coating was lower than the TiCN(2) coating, i.e., there were more defects in the TiCN(3) coating.

3.2. OCP tests

As seen in Fig. 3, after a short penetration process, the TiN and TiCN coatings displayed steady OCPs. Moreover, the OCP increased gradually as carbon concentration increased, which declares the less opportunity of corrosion occurrence for higher carbon contained TiCN coating. The reason for this phenomenon is the more a-CN_x with correspondingly higher electrical resistivity in Table 3.

3.3. Evolution of EIS spectra

The Nyquist plots and corresponding Bode plots of TiCN coatings are illustrated in Fig. 4. All samples displayed incomplete capacitive resistance arcs in Fig. 4a, and the TiN coating exhibited the smallest diameter while the TiCN(2) coating exhibited the biggest one. As seen in Fig. 4b, the TiN coating exhibited the narrowest range of frequency (10⁻²–10¹ Hz) with angle higher than 70°. In contrast, the TiCN(2) coating displayed the broadest range of frequency (10⁻³–10⁴ Hz) with an angle higher than 70°. It is indicated that the TiCN(2) coating would more likely to act as an ideal capacitor during broader frequency range and provided more protection than the other coatings. As for TiCN(3) coating, the similar range of frequency (10⁻²–10⁴ Hz) with an angle higher than 70° was exhibited, but the phase during the media frequency (10⁻¹–10¹ Hz) was very unstable. Just as above-mentioned, the more defects due to a mixture of a-CN_x and a-C in TiCN(3) coating would be the key reason to this phenomenon.

According to the Nyquist and Bode plots shown in Fig. 4 and chi-square values after ZsimpWin software testings, the TiN and TiCN-coated samples could be well depicted by equivalent circuit with two time constants in Fig. 5, which has been used frequently to describe the AC response of a defective non-conducting polymer film on a metallic substrate [38]. In equivalent circuit (EC), electrolyte resistance R_s originates from the ohmic contribution of electrolyte solution between working and reference electrodes; pore resistance R_{po} is related to the coatings' block effect, and will hinder the electrolyte penetration; CPE_{po} is the corresponding coatings' capacitance; R_{ct} is related to charge transfer resistance due to the formation of a double layer of charge at the Si/electrolyte interface, and CPE_{dl} is the corresponding double-layer capacitance. Here, constant phase element is used to represent a non-ideal capacitor, and describe the deviation from the actual capacitive behavior [39]. Its impedance is expressed as:

$$Z_Q = 1/[Y_o(j\omega)^n] \quad (2)$$

where Y_o is capacitance (F cm⁻²), ω is angular frequency (rd/s), and n is CPE power that represents the degree of deviation from a pure capacitor. For n = 1, Q is an ideal capacitor, while for n < 1, Q is non-ideal.

According to the above-mentioned EC, the value of each component is listed in Table 5 after curve is fitted with ZsimpWin software. Overall, the higher R_{ct} (2.56 × 10⁶–6.49 × 10⁶ Ω cm²) of TiCN coatings demonstrates their stronger anti-corrosion abilities than that of the TiN coating. To be specific, due to increasing electrical

Table 5
Characteristics of the equivalent circuit derived from the EIS spectra in SBF.

Coatings	R _s (Ω cm ²)	(CPE-Y _o) _{po} (F cm ⁻²)	(CPE-n) _{po}	R _{po} (Ω cm ²)	(CPE-Y _o) _{dl} (F cm ⁻²)	(CPE-n) _{dl}	R _{ct} (Ω cm ²)
TiN	1.23	1.03 × 10 ⁻⁶	0.878	1.82 × 10 ¹	6.87 × 10 ⁻⁵	0.908	8.88 × 10 ⁵
TiCN(1)	1.35	4.25 × 10 ⁻⁵	0.871	3.46 × 10 ²	1.05 × 10 ⁻⁵	0.887	4.17 × 10 ⁶
TiCN(2)	1.50	2.52 × 10 ⁻⁵	0.998	2.35 × 10 ⁴	3.35 × 10 ⁻⁵	0.921	6.49 × 10 ⁶
TiCN(3)	1.17	1.98 × 10 ⁻⁵	0.999	5.62 × 10 ³	7.50 × 10 ⁻⁵	0.750	2.56 × 10 ⁶

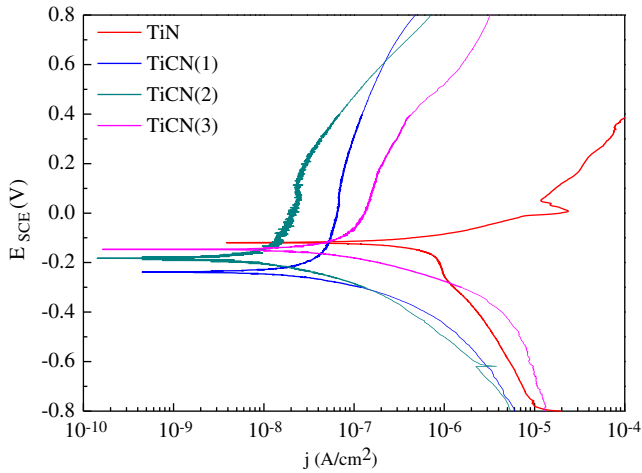


Fig. 6. Polarization curves of TiN and TiCN coatings deposited at different graphite target currents.

Table 6
Results of potentiodynamic polarization tests.

Coatings	E vs SCE (V)	j_{corr} (nA cm^{-2})	β_a (V)	β_c (V)	R_p ($\text{k}\Omega \text{cm}^2$)
TiN	-0.114	561	0.072	0.794	51.1
TiCN(1)	-0.239	44.9	0.470	0.121	930.6
TiCN(2)	-0.181	15.0	0.664	0.111	2753.0
TiCN(3)	-0.151	77.8	0.385	0.103	453.5

resistivity, the R_{ct} of TiN, TiCN(1) and TiCN(2) coatings increased gradually from $8.88 \times 10^5 \Omega \text{cm}^2$ to $6.49 \times 10^6 \Omega \text{cm}^2$. In principle, with a higher electrical resistivity, the TiCN(3) coating should present a higher

R_{ct} as compared with TiCN(1) and TiCN(2) coatings. However, in practice, a lower R_{ct} of $2.56 \times 10^6 \Omega \text{cm}^2$ was obtained for TiCN(3) coating, because another crucial factor of compactness here affects corrosion resistance indirectly. As the above-mentioned, the TiCN(3) coating exhibited a larger standard deviation (3.1 GPa) of hardness, which indicates that more defects exist due to the quaternary mixture of TiN, TiC, a-CN_x and a-C [21]. As a result, the electrolyte is easy to attack the Si wafer by penetrating through these defects. In addition, the highest (CPE-n)_{dl} for TiCN(2) coating and the lowest one for TiCN(3) coating can explain the variation trend of R_{ct} from another perspective.

3.4. Potentiodynamic polarization tests

According to the Tafel extrapolation method, E_{corr} , j_{corr} , β_a and β_c had been obtained from polarization curves shown in Fig. 6, and then R_p was calculated by Eq. (1). On the one hand, it is obvious that TiCN coatings exhibited the lower j_{corr} ($15.0\text{--}77.8 \text{ nA cm}^{-2}$) than that (561 nA cm^{-2}) of TiN coating (Table 6), which implies that the corrosion rates of TiCN coatings are lower than that of the TiN coating. On the other hand, the higher R_p ($453.5\text{--}2753.0 \text{ k}\Omega \text{cm}^2$) of TiCN coatings also prove their stronger corrosion resistances to SBF than that of the TiN coating. Besides, it is worth noting that the variation trend of R_p is similar with that of R_{ct} , i.e., the TiCN(2) coating exhibited the highest R_p and R_{ct} simultaneously. Based on this, after polarization tests, the TiCN(2) coating showed smoother surface as compared with the other samples shown in Fig. 7. However, as for TiCN(3) coating, local corrosion occurred with many big corrosion holes, which demonstrates the weaker corrosion resistance to SBF.

4. Conclusion

The influence of low carbon concentrations (0.99 at.%–2.46 at.%) on the electrochemical behavior of TiCN coatings in simulated body fluid

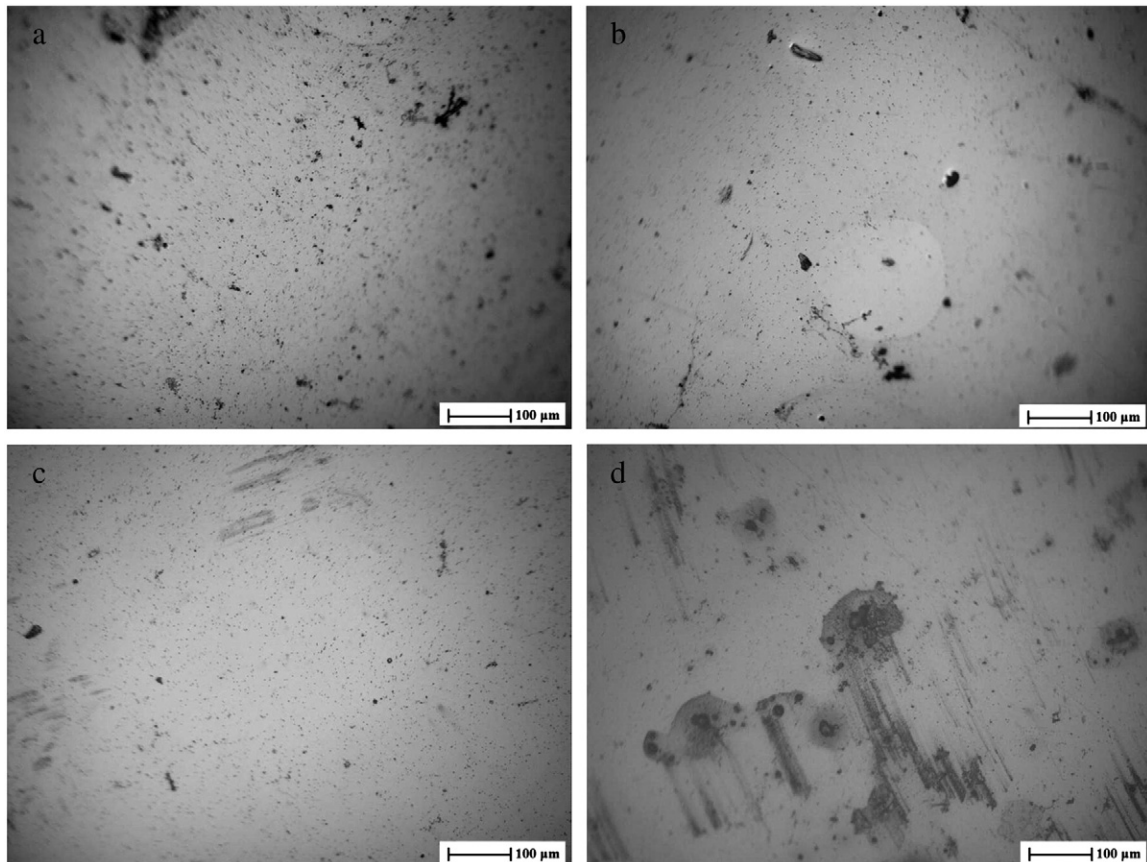


Fig. 7. Optical images of (a) TiN (c) TiCN(1) (e) TiCN(2) (g) TiCN(3) coatings after polarization tests.

(SBF) was investigated via open circuit potential (OCP), electrochemical impedance spectroscopy (EIS) and potentiodynamic polarization tests. Although, after carbon doping, all of the TiCN coatings showed stronger corrosion resistances to SBF than TiN coating, there is a critical carbon concentration for optimal electrochemical performance. In another word, the TiCN(2) coating (2.05 at.% C) with a mixture of TiN, TiC and a-CN_x exhibited the higher electrical resistivity and fewer defects, and therefore, presented the favorable anti-corrosion property in simulated body fluid.

Conflict of interest

None.

Acknowledgment

This work was supported by the National Natural Science Foundation of China (Grant No. 51375231), the Research Fund for the Doctoral Program of Higher Education (Grant No. 20133218110030) and the Project Funded by Priority Academic Program Development of Jiangsu Higher Education Institutions (PAPD). We would like to acknowledge them for their financial support.

References

- [1] D. Gopi, V.C.A. Prakash, L. Kavitha, *Mater. Sci. Eng. C* 29 (2009) 955–958.
- [2] Y. Khelifaoui, M. Kerkar, A. Bali, F. Dalar, *Surf. Coat. Technol.* 200 (2006) 4523–4529.
- [3] K. Nielsen, *Br. Corros. J.* 22 (1987) 272–278.
- [4] S.A. Brown, K. Merritt, *J. Biomed. Mater. Res.* 15 (1981) 479–488.
- [5] H. Placko, S. Brown, J. Payer, *J. Biomed. Mater. Res.* 17 (1983) 655–668.
- [6] V. Singh, K. Marchev, C.V. Cooper, E.I. Meletis, *Surf. Coat. Technol.* 160 (2002) 249–258.
- [7] J. Pellier, J. Geringer, B. Forest, *Wear* 271 (2011) 1563–1571.
- [8] S. Carmignato, M. Spinelli, S. Affatato, E. Savio, *Wear* 270 (2011) 584–590.
- [9] J. Geringer, W. Tatkiwicz, G. Rouchouse, *Wear* 271 (2011) 2793–2803.
- [10] R. Crowninshield, A. Rosemberg, S. Sporer, *Clin. Orthop. Relat. Res.* 443 (2006) 266–272.
- [11] D.F.G. Emery, H.J. Clarke, M.L. Grover, *J. Bone Joint Surg.* 79 (1997) 240–246.
- [12] Z. Bou-Saleh, A. Shahryari, S. Omanovic, *Thin Solid Films* 515 (2007) 4727–4737.
- [13] V. Muthukumar, V. Selladurai, S. Nandhakumar, M. Senthilkumar, *Mater. Des.* 31 (2010) 2813–2817.
- [14] F. Macionczyk, B. Gerold, R. Thull, *Surf. Coat. Technol.* 142–144 (2001) 1084–1087.
- [15] D. Bociaga, K. Mitura, *Diamond Relat. Mater.* 17 (2008) 1410–1415.
- [16] Y.H. Cheng, T. Browne, B. Heckerman, *Surf. Coat. Technol.* 205 (2011) 4024–4029.
- [17] Y.H. Cheng, T. Browne, B. Heckerman, *J. Vac. Sci. Technol. A* 28 (3) (2010) 431–437.
- [18] Y.H. Cheng, T. Browne, B. Heckerman, *Vacuum* 85 (2010) 89–94.
- [19] S.W. Huang, M.W. Ng, M. Samandi, *Wear* 252 (2002) 566–579.
- [20] G.J. Zhang, B. Li, B.L. Jiang, F.X. Yan, D.C. Chen, *Appl. Surf. Sci.* 255 (2009) 8788–8793.
- [21] Q.Z. Wang, F. Zhou, Z.F. Zhou, Y. Yang, Ce Yan, C.D. Wang, W.J. Zhang, L.K.-Y. Li, I. Bello, S.-T. Lee, *Surf. Coat. Technol.* 206 (2012) 3777–3787.
- [22] H.C. Barshilia, M.S. Prakash, A. Poojari, K.S. Rajam, *Trans. Inst. Met. Finish.* 82 (2004) 123–128.
- [23] R.A. Antunes, A.C.D. Rodas, N.B. Lima, O.Z. Higa, I. Costa, *Surf. Coat. Technol.* 205 (2010) 2074–2081.
- [24] S. Sofiane, A. Slimane, A. Ahmet, E. Volkan, *Appl. Surf. Sci.* 295 (2014) 81–85.
- [25] L.F. Senna, C.A. Achetea, T. Hirschb, F.L. Freire Jr., *Surf. Coat. Technol.* 91–95 (1997) 390–397.
- [26] D.G. Liu, J.P. Tu, R. Chen, C.D. Gu, *Surf. Coat. Technol.* 206 (2011) 165–171.
- [27] Q.Z. Wang, F. Zhou, Z.F. Zhou, C.D. Wang, W.J. Zhang, L.K.-Y. Li, S.-T. Lee, *Electrochim. Acta* 112 (2013) 603–611.
- [28] P.J. Li, C. Ohtsuki, T. Kokubo, K. Nakanishi, N. Soga, *J. Am. Ceram. Soc.* 75 (1992) 2094–2097.
- [29] B.A. Boukamp, *J. Electrochem. Soc.* 142 (1995) 1885–1894.
- [30] C. Anandan, V.K. William Grips, V. Ezhil Selvi, K.S. Rajam, *Surf. Coat. Technol.* 201 (2007) 7873–7879.
- [31] I. Dreiling, A. Haug, H. Holzschuh, *Surf. Coat. Technol.* 204 (2009) 1008–1012.
- [32] C. Casiraghi, A.C. Ferrari, J. Robertson, *Phys. Rev. B Condens. Matter* 72 (085401) (2005) 1.
- [33] L. Escobar-Alarcon, V. Medina, E. Camps, S. Romero, M. Fernandez, D. Solis-Casados, *Appl. Surf. Sci.* 257 (2011) 9033–9037.
- [34] L.C. Agudelo, R. Ospina, H.A. Castillo, A. Devia, *Phys. Scr. T131* (2008) 014006.
- [35] H. Liu, Y.H. Jiang, Z.L. Zhan, B.Y. Tang, *Spectrosc. Spectr. Anal.* 29 (2009) 2585–2589 (in Chinese).
- [36] M.S.R.N. Kiran, M. Ghanashyam Krishna, K.A. Padmanabhan, *Appl. Surf. Sci.* 255 (2008) 1934–1941.
- [37] Y.L. Yu, B. Zhang, J.Y. Zhang, *Electrochem. Commun.* 11 (2009) 772–775.
- [38] F. Mansfeld, *J. Appl. Electrochem.* 25 (1995) 187–202.
- [39] C. Liu, Q. Bi, A. Leyland, A. Matthews, *Corros. Sci.* 45 (2003) 1243–1256.